Anti- and De-Icing Behaviors of Superhydrophobic Fabrics

Yuyang Liu, Dong Song and Chang-Hwan Choi * [ID]

Department of Mechanical Engineering, Stevens Institute of Technology, Hoboken, NJ 07030, USA;
tcliuyy@gmail.com (Y.L.); dsong3@stevens.edu (D.S.)
* Correspondence: cchoi@stevens.edu; Tel.: +1-201-216-5579

check for
updates

Abstract: This paper reports the application of superhydrophobic coatings on cotton fabrics and their functionalities for anti- and de-icing efficacy. Superhydrophobic cotton fabrics with different water-repellent properties have been achieved by decorating the surface of pristine cotton fibers with ZnO structures of varying sizes and shapes through an in situ solution growth process, followed by the treatment of the surface with low-surface-energy coating such as Teflon. The surface morphology of the treated cotton fabrics was characterized using scanning electron microscopy (SEM). The surface wettability of the treated fabrics was evaluated through the measurement of static contact angle (SCA), contact angle hysteresis (CAH), and sliding angle (SA) of a water droplet. The anti- and de-icing behaviors of the treated fabrics were evaluated through both static (sessile droplet) and dynamic (spraying) tests. The results show that the superhydrophobic fabric with a higher SCA and the lower CAH/SA has superior anti- and de-icing behaviors in both the static and dynamic conditions. Compared to hard substrates, the soft, flexible, and porous (air-permeable) superhydrophobic fabrics can lead to broader applicability of textile-based materials for the design and fabrication of anti- and de-icing materials. Furthermore, the multi-scale surface structures of fabrics (fibers, yarns, and weaving constructions) combining with the hierarchical micro-nanostructures of the ZnO coating provides an ideal platform for anti-icing studies.

Keywords: anti-icing; de-icing; fabrics; nanostructures; superhydrophobic

1. Introduction

Superhydrophobic materials and surfaces [1–4] have attracted great interest because of their extreme water-repellent surface property for many potential applications including self-cleaning [5–7], hydrodynamic friction reduction [8–10], anti-icing [11–14], anticorrosion [15–18], biotechnology [19–21], thermal systems [22–25], and micro- and nanodevices [26–28]. In particular, previous works on the use of superhydrophobic surfaces as anti-icing coatings have demonstrated that superhydrophobic surfaces have the capability to reduce or even prevent the accumulation and formation of snow and ice on hard solid surfaces [11–14]. Aizenberg's team [13] designed nanostructured surfaces that could be used for anti-icing applications. Their experimental results show that highly ordered superhydrophobic materials can be designed to remain entirely ice-free down to circa −25 to −30 °C, due to their ability to repel impacting water before ice nucleation occurs. However, the limitations of the superhydrophobic surfaces on the anti-icing applications have also been reported recently. Due to the complexity of water property, frost nucleation within structured surfaces is hardly avoided considering the fact that evaporation accompanies the freezing process and change the surface behavior, which will even increase the adhesion force of ice on the roughened superhydrophobic surfaces [12,29]. Gao et al. indicated that the anti-icing competence of superhydrophobic surfaces depended not only on the superhydrophobicity but also the size of the

surface roughness [11]. To prevent icing formation, nano-sized structures, smaller than the size of the critical nucleus of ice, has to be introduced on the superhydrophobic surfaces.

To enhance the hydrophobicity of a surface, the combination of the surface texturing and chemical modification has been widely applied based on the wetting theory of Cassie–Baxter model [30]. Recently, it has been demonstrated that by controlling the physical property of the substrate, surface flexibility for example, the superhydrophobicity can be significantly enhanced under dynamic conditions [31]. Even though many engineering and natural surfaces are flexible [32], the anti- and de-icing property of superhydrophobic structures on soft, flexible, and porous textile surfaces still remains unexplored. In this paper, we demonstrate the synthesis of superhydrophobic fabrics which are soft, flexible, and porous, and their anti- and de-icing properties under both static (Sessile drop) and dynamic (impacting supercooled droplet) conditions.

2. Experimental Setup

2.1. Preparation of Cotton Fibers Decorated with ZnO Structures

Cotton fibers decorated with ZnO structures were prepared by treating pristine cotton fabric with an in situ hydrothermal growth process. The details of this procedure are schematically shown in Figure 1. Cotton fabrics were kept in deionized water at 90 °C with stirring for 30 min to dissolve impurities. Then, the cotton fabric samples were rinsed with tap water for 2 min to remove the impurities and then dried at 120 °C in a pre-heated oven for 30 min. The cotton fabrics were cut into small pieces (10 cm × 20 cm) and then the specimens were placed into a 1000-mL beaker containing bulk growth solution with equal molar amount of zinc nitrate hexahydrate (99%) and hexamethylenetetramine (97%). The bulk growth solution together with the cotton samples were heated to 90 °C at the rate of 10 °C/min and then kept at 90 °C for the growth of ZnO structures. Cotton fibers with four different surface structures were designed to achieve different surface wettabilities. The size and shape of ZnO structures decorated on the fiber surface were controlled by growth time and the addition of surfactant sodium dodecyl sulfate (SDS). Figure 1b shows the schematic of the cotton fiber decorated with ZnO microparticles, where the growth time is limited to be short (10 min) with no use of surfactant. In comparison, Figure 1c,d show the schematic of the cotton fiber decorated with ZnO nanostructures. The longer growth time (30 min) with the use of surfactant is employed for the growth of ZnO nanowire structures on the surface of cotton fiber (Figure 1c). After the growth of the nanowire structures for the first layer, the samples were taken out from the reaction solution, rinsed with deionized water four times (by dipping the sample in 500 mL deionized water) to remove surface residuals. Then, the samples were put back to the reaction solution for the growth of nanoflower structures. Additional growth time (60 min) with the use of surfactant was employed for the growth of nanoflower structures on top of the nanowire structures (Figure 1d). The cotton fabric sample was taken out from the bulk solution after the modulated process time and condition. The samples were then rinsed with tap water and dried at 120 °C for 30 min. The ZnO structures grown on the cotton fibers were characterized with field-emission scanning electron microscope (FE-SEM, JEOL, Tokyo, Japan).
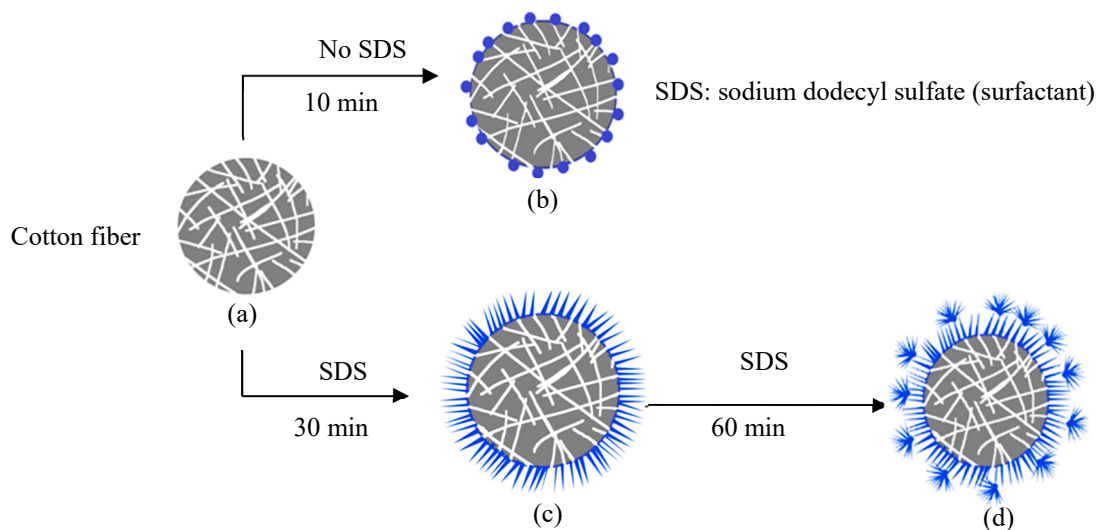
Figure 1. Decoration of cotton fibers with ZnO structures through an in situ solution growth process. (**a**) Pristine cotton fiber; (**b**) Cotton fiber coated with ZnO microparticles; (**c**) Cotton fiber coated with ZnO nanowire structures; (**d**) Cotton fiber coated with nanoflower-over-nanowire structures.

2.2. Hydrophobic Coating of Cotton Fabric Samples with Teflon

All the cotton samples were hydrophobized with Teflon coating by dipping the cotton samples in the solution of 0.1% Teflon AF 1600 [33] in FC-40 (3M™ Fluorinert™ Electronic Liquid) for 2 min and then dried at 120 °C in a pre-heated oven for 30 min in an oven.

2.3. Evaluation of Surface Wettability

The surface wettability of the cotton fabric samples was evaluated by measuring the contact angle (CA), the contact angle hysteresis (CAH), and the sliding angle (SA) of a sessile droplet of water at room condition with a custom-made goniometer system. For the CA, static contact angle (SCA), advancing contact angle (ACA), and receding contact angle (RCA) were measured. The ACA and the RCA were measured during the sliding tests. The CAH was evaluated as the difference between the ACA and RCA.

2.4. Evaluation of Anti-Icing and De-Icing Properties

The anti-icing behavior of the cotton fabric samples was evaluated by both static and dynamic tests. In the static test, three water droplets (volume around 0.1 mL) were first placed on the cotton fabric surfaces and then kept at −18 °C in a biochemical freezer to allow icing. Several parallel experiments were conducted and the ice beads formed on the fabric surfaces were crushed with tweezers to check the fully frozen state. After the fully frozen state, the samples were placed on a 45°-slope plate and exposed to a room condition (25 °C and 50% relative humidity (RH)) immediately to test subsequent de-icing behavior. In the dynamic test, a spraying test method was employed, based on AATCC (American Association of Textile Chemists and Colorists) Test Method 22-2005. The schematic of the instrument for the spraying test is shown in Figure 2. First, the fabric sample was placed on a 45°-slope plate. Then, 50 mL supercooled water was sprayed onto the fabric surfaces at a height of 15 cm. The ice formation and mobility on the surfaces were measured. The supercooled water was prepared by pouring double distilled water into clean plastic bottles and then kept the bottles in the freezer at temperature of −4 °C for 2–3 h. The exact time for the formation of supercooled water depends on the temperature of the freezer. In order to ensure the formation of supercooled water, a control bottle containing tap water was also placed into the freezer at the same time. When the tap water freezes, it guarantees that the double distilled water is supercooled. The supercooled

water bottles were kept intact until the spraying tests, because supercooled water can freeze easily when disturbed.
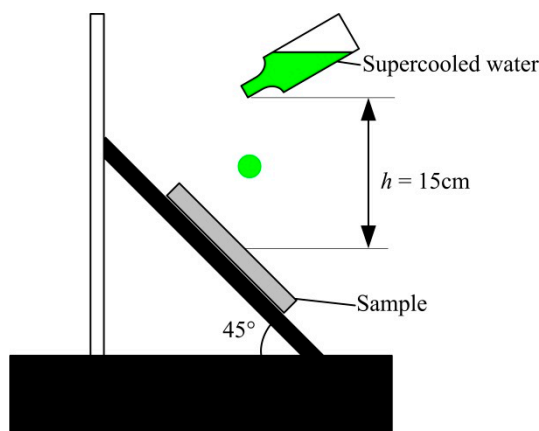

Figure 2. Schematic diagram of the dynamic spraying test.

3. Results and Discussion

3.1. ZnO Surface Structures Grown on Cotton Fibers

Figure 3 shows the SEM images of the cotton fibers prepared using the process described in Figure 1. The structures of the pure cotton fibers coated with Teflon is shown in Figure 3a, indicating that a cotton fiber has a relatively smooth surface and a characteristic diameter of ~20 μm. Figure 3b shows the Teflon-coated ZnO microstructures grown on the cotton fibers following the process shown in Figure 1b. In this case, there is a layer of secondary microstructures, distributed randomly and sparsely on the microfibers of cotton. The shapes of secondary microstructures are spherical and their sizes (diameters) range between 1 and 2 μm. The formation of the random microstructures results from the relatively poor control of crystallization in the pure aqueous solution without any precursor solution. In contrast, with the aid of surfactant such as SDS, ZnO with different shapes such as rod-like, wire-like, and spherical nanoparticles can be obtained by varying the amount of surfactant molecules, reaction time, and reaction temperatures [34–36]. Figure 3c shows the Teflon-coated ZnO nanostructures grown on the cotton fibers treated with the bulk growth solution containing 0.1% SDS for 30 min (following the process shown in Figure 1c). The secondary ZnO microstructures transformed to be nanowires (typical diameter of ~200 nm) which are now dense and fully covering on the cotton microfibers. The result demonstrates that the elongated growth time with the use of surfactant (0.1% SDS) allows the reduction of the size of ZnO particles and makes them have the shape of nanowire morphology and fully cover the surface. The origin of the morphology difference is due to the chemical interaction between the ZnO seed crystal and the ions produced by the ionization of the SDS [36,37]. The negatively charged SDS ions create micelles around the ZnO seeds during the reaction which causes the supplement of Zn^{2+} for ZnO seeds to be insufficient. As a result, the chemically activated lattice defects form on the surface and serve as nucleation sites of the growth of ZnO rods in random directions. If we extend the growth time to 60 min while keeping the concentration of surfactant (SDS) the same with the previous one as 0.1% (following the process shown in Figure 1d), the third layer of smaller nanowires forms on top of the secondary nanowires, resulting in a hierarchical morphology of nanoflower structures over the nanowires as clearly shown in Figure 3d. The diameter of the nanoflower morphology within the thirdly-grown layer is around 20–50 nm, having sharper tips and much smaller size than the first-grown nanowire structures. The results shown in Figure 3 illuminate that cotton fabrics decorated with the ZnO structures of various sizes and shapes can be conveniently achieved by using the in-situ hydrothermal growth process with the modulation of the growth time and the use of surfactant. The ZnO coating is reportedly durable to sustain the

superhydrophobicity even when being immersed in a hydrochloric acid or sodium hydroxide solution for several hours [38–40].
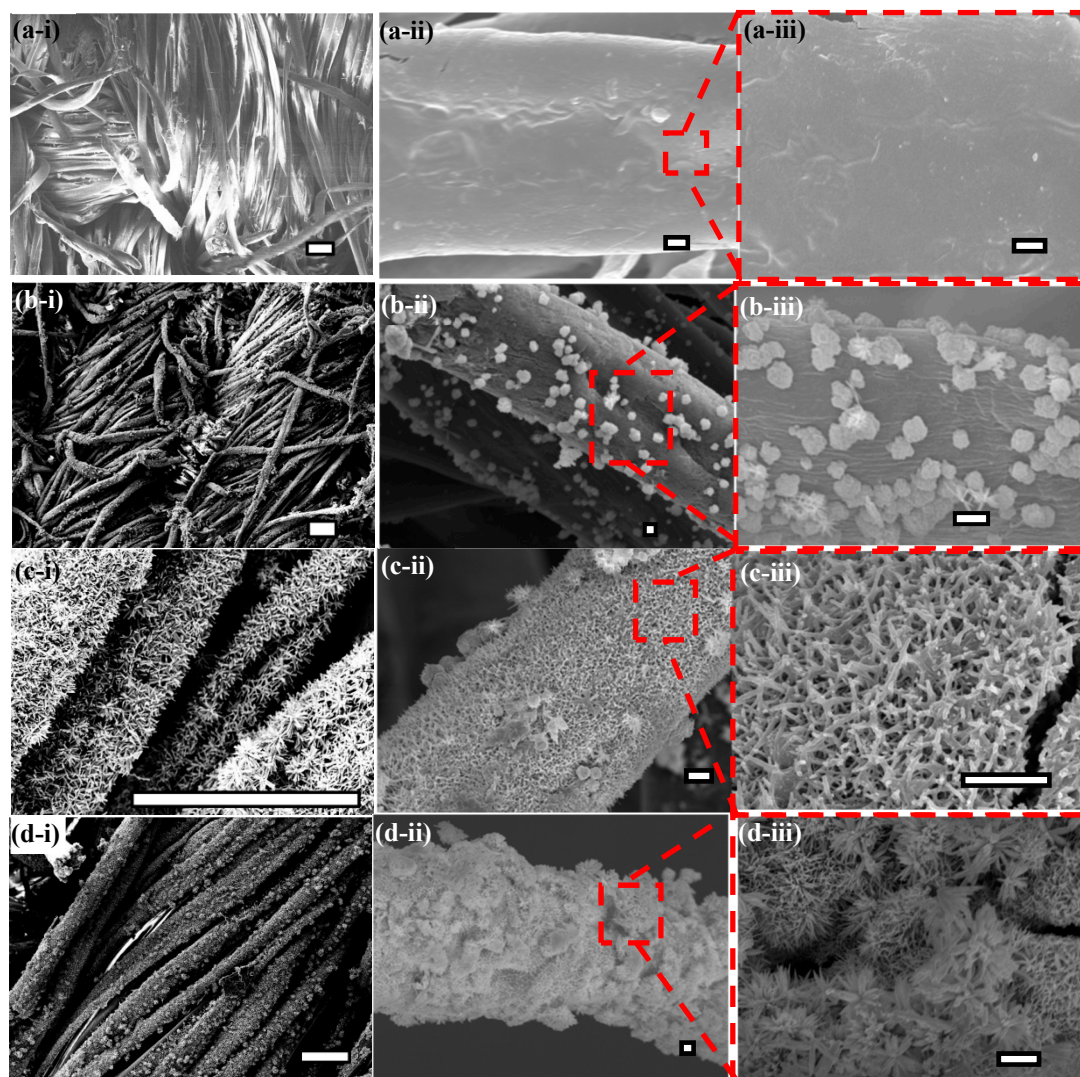

Figure 3. SEM images of cotton fibers decorated with different ZnO structures. (**a**) Pure pristine cotton fabric coated with Teflon; (**b**) Cotton fabric decorated with a secondary micro-sized layer of ZnO microparticles followed by Teflon coating; (**c**) Cotton fabric decorated with a secondary nano-sized layer of ZnO nanowires followed by Teflon coating; (**d**) Cotton fabric decorated with hierarchical tri-layers composed of the ZnO nanoflower-over-nanowire structures followed by Teflon coating. The scale bar in each image in the first column (**i**) indicates 30 μm; while those in the second (**ii**) and third (**iii**) columns indicate 1 μm.

3.2. Surface Wettability of Treated Cotton Fabrics

The Teflon-coated cotton fabrics decorated with the different surface morphologies of the ZnO structures allow the surfaces to exhibit different surface wettabilities. The surface wettabilities of the treated cotton fabrics were evaluated through the measurement of SCA, ACA, RCA, CAH, and SA, as shown in Figure 4. The results are summarized in Table 1, where the average values were used based on five parallel measurements. The results show that the CA of a water droplet on the hydrophobized cotton fabric increases gradually with the increase of the surface roughness provided by the decoration of ZnO structures, whereas the CAH and the SA decrease with the increase of the surface roughness. In the estimation of the CAH, the ACA did not change much regardless of the surface roughness, whereas

the RCA changed significantly with the increase of the surface roughness and mainly affected the CAH. The results indicate that the surface becomes more slippery (or less frictional) with the increase of the surface roughness. It is attributed to the fact that more air is entrained between the hydrophobic rough structures and the water drop has less contact with the solid surface with the increase of the surface roughness, following the Cassie–Baxter superhydrophobic wetting state [30], as depicted in Figure 5.
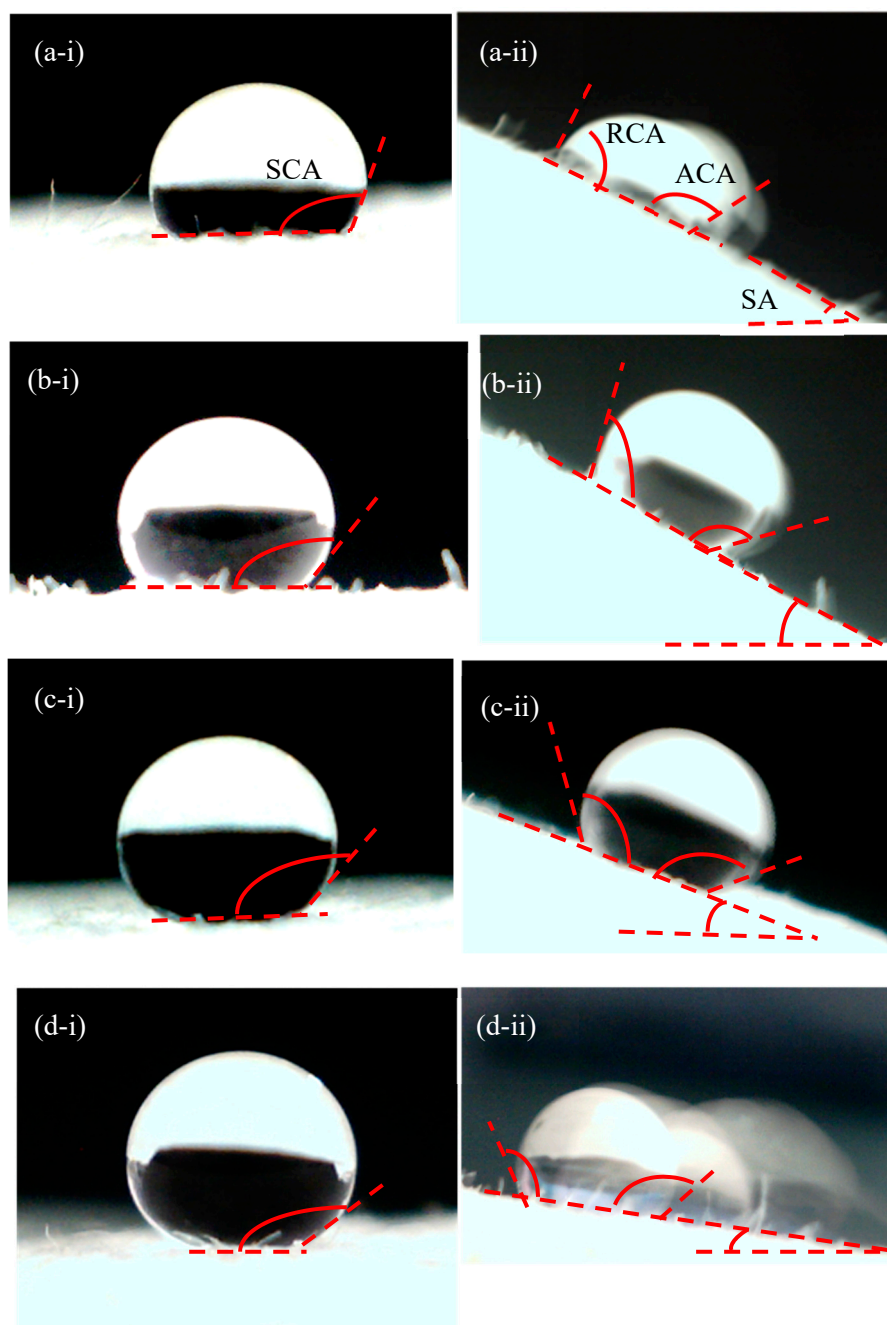

Figure 4. Surface wettability of treated cotton fabrics. (**a**) Pure pristine cotton fabric coated with Teflon; (**b**) Cotton fabric decorated with a secondary micro-sized layer of ZnO microparticles followed by Teflon coating; (**c**) Cotton fabric decorated with a secondary nano-sized layer of ZnO nanowires followed by Teflon coating; (**d**) Cotton fabric decorated with hierarchical tri-layers composed of the ZnO nanoflower-over-nanowire structures followed by Teflon coating. The first column (**i**) shows the static contact angle (SCA) of a water droplet; The second column (**ii**) shows the sliding angle (SA) and the advancing contact angle (ACA) and the receding contact angle (RCA) at the sliding.
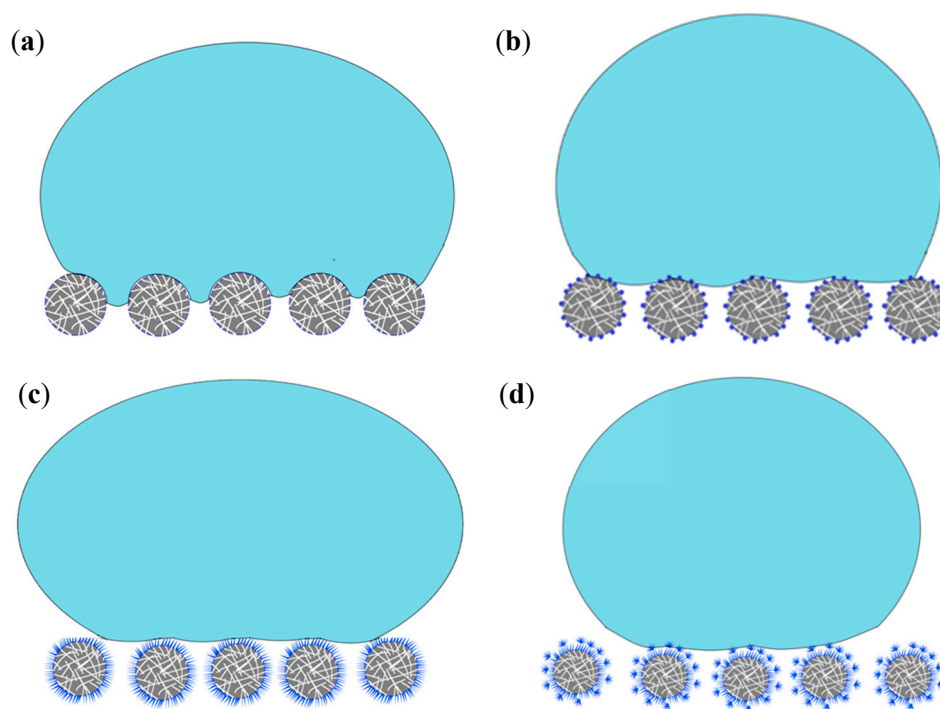
Figure 5. Schematics of the wetting states of water droplets on treated cotton fabrics. (**a**) Pure pristine cotton fabric coated with Teflon; (**b**) Cotton fabric decorated with a secondary micro-sized layer of ZnO microparticles followed by Teflon coating; (**c**) Cotton fabric decorated with a secondary nano-sized layer of ZnO nanowires followed by Teflon coating; (**d**) Cotton fabric decorated with hierarchical tri-layers composed of the ZnO nanoflower-over-nanowire structures followed by Teflon coating.

Table 1. Summary of the wettability of treated cotton fabrics.

Samples	SCA (°)	ACA (°)	RCA (°)	CAH (°)	SA (°)
(a)	137	142	98	44	36
(b)	143	148	113	35	27
(c)	151	156	138	18	22
(d)	153	162	149	13	9

3.3. Anti-Icing and De-Icing Testing under Static Condition

Figure 6 presents the anti-icing and de-icing behaviors of the superhydrophobic cotton fabrics measured in a static condition. The initial water droplets (~0.1 mL, column i in Figure 6) were all frozen on the four different types of the surfaces with not significant difference in the freezing time. When these cotton fabrics together with the frozen ice-beads forming on the surfaces were exposed to a room condition (25 °C and 50% RH) on the 45°-slope plate (column ii in Figure 6), the ice beads on all of the fabric surfaces did not slide off the surfaces but initially stuck to the fabrics. After 5 s (column iii in Figure 6), the ice beads started to melt on the surface. Whereas all the ice beads formed on the pure Teflon-coated pristine cotton fabric (Figure 6(a-iii)), the Teflon-coated cotton fabric decorated with a secondary ZnO microstructures (Figure 6(b-iii)), and the Teflon-coated cotton fabric decorated with a secondary ZnO nanostructures (Figure 6(c-iii)) remained on the surfaces with melting, some ice bead formed on the Teflon-coated cotton fabric decorated with hierarchical tri-layers composed of the ZnO nanoflower-over-nanowire structures (Figure 6(d-iii)) started to slide off the surface. After 15 s (column iv in Figure 6), some ice beads on the Teflon-coated pristine cotton fabric (Figure 6(a-iv)) started to slide off the surface, whereas others remained on the surface. In the case of the Teflon-coated cotton fabric decorated with a secondary ZnO microstructures (Figure 6(b-iv)), the similar behaviors were shown except that there were some wetting spots left on the surface after the

sliding-off. The secondary microstructures (1–2 μm in size) sparsely and randomly distributed over the cotton fibers allowed water to penetrate into the microstructures under the cold conditions, resulting in the local Wenzel state on the layer of secondary microstructures [41] and making the droplets subject to the rose-petal effect [42] with the increase of the pinning and adhesion force. In the cases of the Teflon-coated cotton fabrics decorated with the secondary ZnO nanostructures (Figure 6(c-iv)) and the hierarchical tri-layers composed of the ZnO nanoflower-over-nanowire structures (Figure 6(d-iv)), all the ice beads slid off the surfaces. Whereas many small wetting spots were left on the Teflon-coated cotton fabrics decorated with the secondary ZnO nanostructures (Figure 6(c-iv)) after the sliding-off, there were few on the Teflon-coated cotton fabrics decorated with the hierarchical tri-layers composed of the ZnO nanoflower-over-nanowire structures (Figure 6(d-iv)). Figure 6b,c imply that micro- and nanostructures larger than ∼200 nm cannot avoid water penetration into structures under the cold conditions. According to the classical nucleation theory, the radius of the critical nucleus is as small as 22 nm at ∼−20 °C [11], which is much smaller than the characteristic size of the nano-wires of the surface (∼200 nm) shown in Figure 3c. During the freezing process, the formation of ice nucleus within the nanowires is still energetically favorable and the Wenzel state cannot be avoided. However, on the surface with hierarchical morphologies shown in Figure 3d, the nanoflower over nanowires are smaller than the nanowires (only tens of nanometers). Thus, ice cannot easily form within the nanostructures and the Cassie–Baxter state maintains even the temperature decrease to as low as −18 °C. The results demonstrate that although ice can still form and stick to the superhydrophobic fabrics with micro-sized structures under the static condition, the superhydrophobic fabric surface with nano-sized structures, especially the one with hierarchical morphologies, can show both superhydrophobicity with high CA, low CAH, and a low SA, and the efficient de-icing properties.

3.4. Anti-Icing and De-Icing Testing under Dynamic Condition

Figure 7 shows the results of anti-icing and de-icing behaviors measured in a dynamic condition with the spray test as illustrated in Figure 2. When a supercooled water droplet impacts on a surface, it instantaneously freezes along with a recalescent stage. Due to the release of latent heat of the flash freezing, only ∼20% of the liquid droplet freezes into ice and the rest turns to ice-water mixture with a jump of the temperature to 0 °C [29]. More importantly, evaporation and the resulting condensation occur during the freezing of the supercooled water. The first column (i) of Figure 7 shows that ice formed and accumulated on the surfaces after spraying the supercooled water (50 mL) on the cotton fabric samples tilted at 45°. The second and the third columns (ii and iii, respectively) of Figure 7 show the water remaining on the surfaces after being exposed to a room condition (25 °C and 50% RH) with a gradual melting for 5 and 10 s, respectively. On the pure Teflon-coated pristine cotton fabric (Figure 7a), the water droplet with a small size was melted and slid off the surface first, whereas that with a large size still remained on the surface even after 10 s. Similar behaviors were shown on the Teflon-coated cotton fabric decorated with a secondary micro-sized layer of ZnO microparticles (Figure 7b). Since the tilted angle of the surface is 45°, larger than the sliding angle (SA) under the Cassie–Baxter state (Table 1), the contradiction clearly indicates that the Wenzel state exists during the freezing of the supercooled droplet. In the case of the Teflon-coated cotton fabric decorated with a secondary nano-sized layer of ZnO nanowires (Figure 7c), most of the water slid off the surface after 10 s, although some of them remained on the surface only after 5 s. In the case of the Teflon-coated cotton fabric decorated with hierarchical tri-layers composed of the ZnO nanoflower-over-nanowire structures (Figure 7d), most of the water slid off the surface after 5 s, taking away the ice accumulated on the surface and leaving a clean surface. Even though the supercooled droplet freezes in an extremely fast speed as soon as it comes in contact with the surface, the intense evaporation of water vapor results in the formation of frost within the surface structures, which will affect the surface behavior. It has been demonstrated that microstructures cannot avoid frost formation due to vapor deposition [12]. This is in agreement with our experiments that the mobility of the frozen droplet decreased or disappeared on the microstructured superhydrophobic surfaces. On the nanostructured surfaces, especially the

nanoflower-over-nanowire structures, ice nucleus can significantly be avoided within the structures due to the relative small size to that of ice nucleus. Therefore, the Cassie–Baxter state as well as the high mobility of the molten droplet are insured in our experiments. The results reveal that the nanostructures of the superhydrophobic cotton fabric can insure the superhydrophobicity and the effective anti/de-icing properties even after the fast freezing of a deeply cooled water droplet.
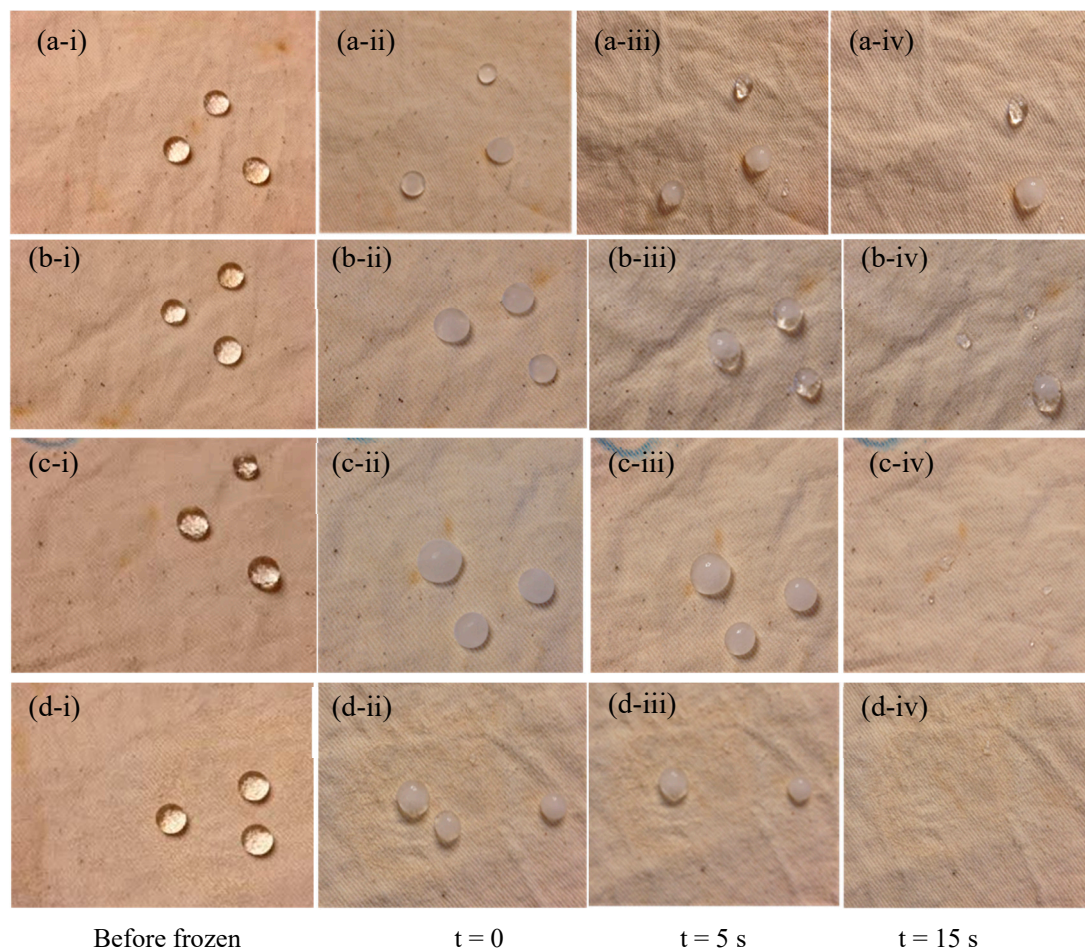

Figure 6. Anti-icing and de-icing behaviors measured in a static condition. (**a**) Pure pristine cotton fabric coated with Teflon; (**b**) Cotton fabric decorated with a secondary micro-sized layer of ZnO microparticles followed by Teflon coating; (**c**) Cotton fabric decorated with a secondary nano-sized layer of ZnO nanowires followed by Teflon coating; (**d**) Cotton fabric decorated with hierarchical tri-layers composed of the ZnO nanoflower-over-nanowire structures followed by Teflon coating. The first column (**i**) shows the initial water droplets placed on horizontally leveled surfaces before freezing; The second column (**ii**) shows the fully frozen water droplets on the leveled surfaces; The third column (**iii**) and the fourth column (**iv**) show the water droplets remaining on the surfaces after the surfaces were tilted at 45° and exposed to a room condition (25 °C and 50% RH) for 5 and 15 s, respectively.
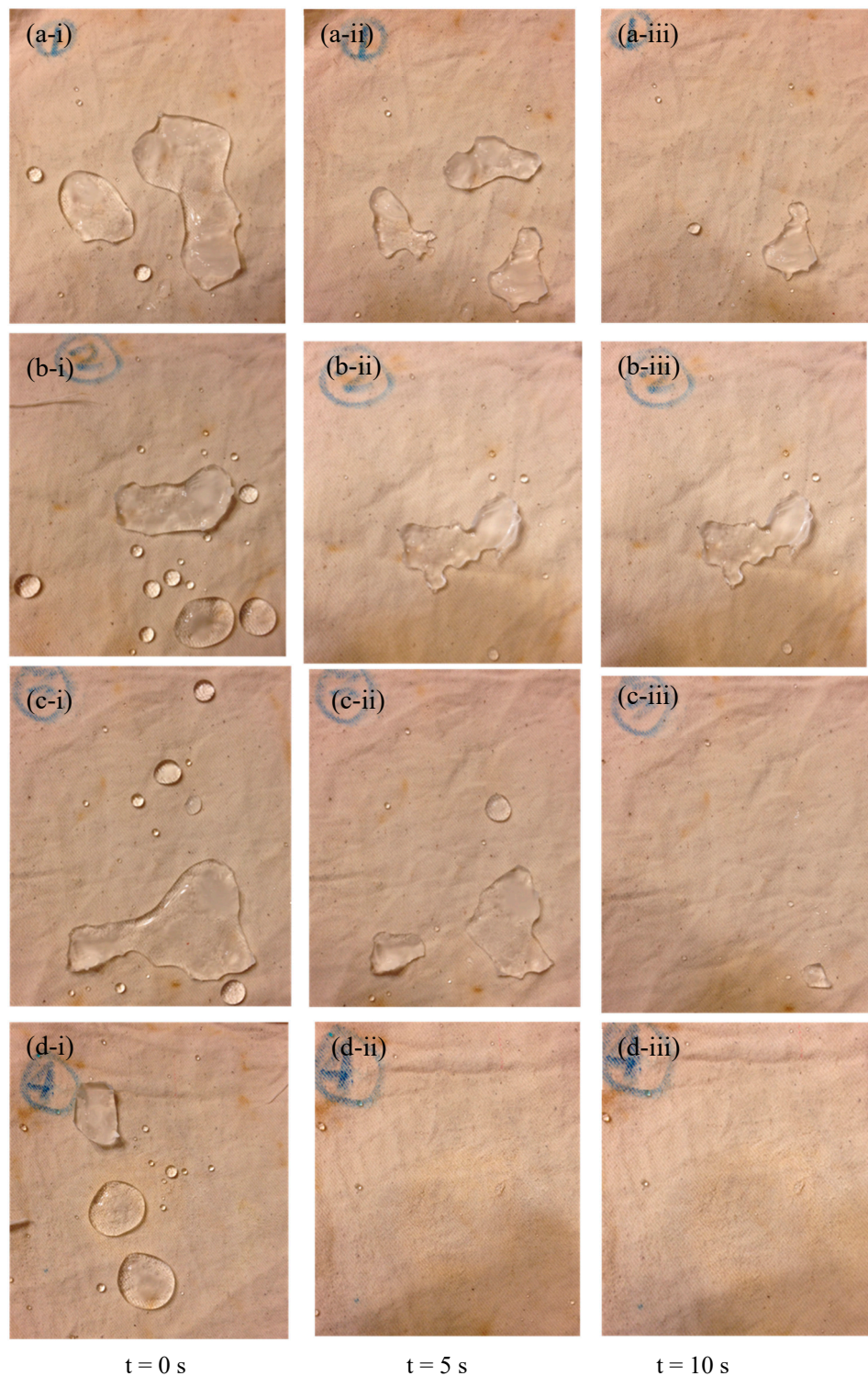
Figure 7. Anti-icing and de-icing behaviors measured in a dynamic condition. (**a**) Pure pristine cotton fabric coated with Teflon; (**b**) Cotton fabric decorated with a secondary micro-sized layer of ZnO microparticles followed by Teflon coating; (**c**) Cotton fabric decorated with a secondary nano-sized layer of ZnO nanowires followed by Teflon coating; (**d**) Cotton fabric decorated with hierarchical tri-layers composed of the ZnO nanoflower-over-nanowire structures followed by Teflon coating. The first column (**i**) shows the initial water left on the 45 °-tilted surfaces after spraying 50-mL supercooled water; The second column (**ii**) and the third column (**iii**) show the water remaining on the surfaces after the surfaces were further exposed to a room condition (25 °C and 50% RH) for 5 and 10 s, respectively. The initial water volume is 50 mL.

4. Conclusions

The anti-icing and de-icing properties of superhydrophobic cotton fabrics with different surface morphologies were examined under both static (sessile droplet) and dynamic (spraying) conditions. The fabric with a higher contact angle and a lower sliding angle or lower contact angle hysteresis to liquid water exhibited more effective anti-icing and de-icing properties. While the anti-icing effects (e.g., delay of ice formation and less amount of ice accretion) were primarily shown in the dynamically loaded condition (spraying), a similar de-icing capability was shown in both the statically loaded and the dynamically impinged water droplets. The significance of this work is that the anti-icing and the de-icing behaviors of superhydrophobic fabrics were studied for the first time, demonstrating that nanostructured superhydrophobic fabrics also have great potential for the anti- and de-icing surfaces. In comparison with conventional superhydrophobic surfaces made on hard substrates, the soft and flexible superhydrophobic fabrics are porous and air-permeable materials that can provide and sustain air between water/fabric interfaces more effectively, which may lead to broader applicability of textile-based materials for the design and fabrication of anti- and de-icing materials.

Author Contributions: Supervision, C.-H.C.; Conceptualization, Y.L. and C.-H.C.; Methodology, validation, and investigation, Y.L.; Date analysis, Y.L. and D.S.; Writing, Y.L., D.S., and C.-H.C.

Conflicts of Interest: The authors declare no conflict of interest.

References

1. Nakajima, A.; Hashimoto, K.; Watanabe, T. Recent Studies on Super-Hydrophobic Films. *Monatsh. Chem.* **2001**, *132*, 31–41. [CrossRef]
2. Lafuma, A.; Quere, D. Superhydrophobic States. *Nat. Mater.* **2003**, *2*, 457–460. [CrossRef] [PubMed]
3. Roach, P.; Shirtcliffe, N.J.; Newton, M.I. Progress in Superhydrophobic Surface Development. *Soft Matter* **2008**, *4*, 224–240. [CrossRef]
4. Bocquet, L.; Lauga, E. A Smooth Future? *Nat. Mater.* **2011**, *10*, 334–337. [CrossRef] [PubMed]
5. Blossey, R. Self-Cleaning Surfaces-Virtual Realities. *Nat. Mater.* **2003**, *2*, 301–306. [CrossRef] [PubMed]
6. Fürstner, R.; Barthlott, W.; Neinhuis, C.; Walzel, P. Wetting and Self-Cleaning Properties of Artificial Superhydrophobic Surfaces. *Langmuir* **2005**, *21*, 956–961. [CrossRef] [PubMed]
7. Liu, Y.; Xin, J.H.; Choi, C.-H. Cotton Fabrics with Single-Faced Superhydrophobicity. *Langmuir* **2012**, *28*, 17426–17434. [CrossRef] [PubMed]
8. Lee, C.; Choi, C.-H.; Kim, C.-J. Superhydrophobic Drag Reduction in Laminar Flows: A Critical Review. *Exp. Fluids* **2016**, *57*, 176. [CrossRef]
9. Aljallis, E.; Sarshar, M.A.; Datla, R.; Sikka, V.; Jones, A.; Choi, C.-H. Experimental Study of Skin Friction Drag Reduction on Superhydrophobic Flat Plates in High Reynolds Number Boundary Layer Flow. *Phys. Fluids* **2013**, *25*, 025103. [CrossRef]
10. Song, D.; Song, B.; Hu, H.; Du, X.; Du, P.; Choi, C.-H.; Rothstein, J.P. Effect of a Surface Tension Gradient on the Slip Flow along a Superhydrophobic Air-Water Interface. *Phys. Rev. Fluids* **2018**, *3*, 033303. [CrossRef]
11. Gao, L.; Jones, A.K.; Sikka, V.K.; Wu, J.; Gao, D. Anti-Icing Superhydrophobic Coatings. *Langmuir* **2009**, *25*, 12444–12448.
12. Kripa, K.V.; Tao, D.; Smith, J.D.; Ming, H.; Nitin, B. Frost Formation and Ice Adhesion on Superhydrophobic Surfaces. *Appl. Phys. Lett.* **2010**, *97*, 234102. [CrossRef]
13. Mishchenko, L.; Hatton, B.; Bahadur, V.; Taylor, J.A.; Krupenkin, T.; Aizenberg, J. Design of Ice-Free Nanostructured Surfaces Based on Repulsion of Impacting Water Droplets. *ACS Nano* **2010**, *4*, 7699–7707. [CrossRef] [PubMed]
14. Sarshar, M.A.; Swarctz, C.; Hunter, S.; Simpson, J.; Choi, C.H. Effects of Contact Angle Hysteresis on Ice Adhesion and Growth on Superhydrophobic Surfaces under Dynamic Flow Conditions. *Colloid Polym. Sci.* **2013**, *291*, 427–435. [CrossRef]

15. Liu, K.; Zhang, M.; Zhai, J.; Wang, J.; Jiang, L. Bioinspired Construction of Mg-Li Alloys Surfaces with Stable Superhydrophobicity and Improved Corrosion Resistance. *Appl. Phys. Lett.* **2008**, *92*, 183103. [CrossRef]
16. Zhang, F.; Zhao, L.; Chen, H.; Xu, S.; Evans, D.G.; Duan, X. Corrosion Resistance of Superhydrophobic Layered Double Hydroxide Films on Aluminum. *Angew. Chem. Int. Ed.* **2008**, *47*, 2466–2469. [CrossRef] [PubMed]
17. Jeong, C.; Lee, J.; Sheppard, K.; Choi, C.-H. Air-Impregnated Nanoporous Anodic Aluminum Oxide Layers for Enhancing the Corrosion Resistance of Aluminum. *Langmuir* **2015**, *31*, 11040–11050. [CrossRef] [PubMed]
18. Lee, J.; Shin, S.; Jiang, Y.; Jeong, C.; Stone, H.A.; Choi, C.-H. Oil-Impregnated Nanoporous Oxide Layer for Corrosion Protection with Self-Healing. *Adv. Funct. Mater.* **2017**, *27*, 1606040. [CrossRef]
19. Ressine, A.; Marko-Varga, G.; Laurell, T.; El-Gewely, M.R. Porous Silicon Protein Microarray Technology and Ultra-/Superhydrophobic States for Improved Bioanalytical Readout. *Biotechnol. Annu. Rev.* **2007**, *13*, 149–200. [PubMed]
20. Choi, C.-H.; Kim, C.-J. Droplet Evaporation of Pure Water and Protein Solution on Nanostructured Superhydrophobic Surfaces of Varying Heights. *Langmuir* **2009**, *25*, 7561–7567. [CrossRef] [PubMed]
21. Hizal, F.; Rungraeng, N.; Lee, J.; Jun, S.; Busscher, H.J.; van der Mei, H.C.; Choi, C.-H. Nanoengineered Superhydrophobic Surfaces of Aluminum with Extremely Low Bacterial Adhesivity. *ACS Appl. Mater. Int.* **2017**, *9*, 12118–12129. [CrossRef] [PubMed]
22. Xu, W.; Choi, C.-H. Effects of Surface Topography and Colloid Particles on the Evaporation Kinetics of Sessile Droplets on Superhydrophobic Surfaces. *J. Heat Transf.* **2012**, *134*, 051022–051027. [CrossRef]
23. Miljkovic, N.; Enright, R.; Wang, E.N. Effect of Droplet Morphology on Growth Dynamics and Heat Transfer during Condensation on Superhydrophobic Nanostructured Surfaces. *ACS Nano* **2012**, *6*, 1776–1785. [CrossRef] [PubMed]
24. Liu, Y.; Choi, C.-H. Condensation-Induced Wetting State and Contact Angle Hysteresis on Superhydrophobic Lotus Leaves. *Colloid Polym. Sci.* **2013**, *291*, 437–445. [CrossRef]
25. Betz, A.R.; Jenkins, J.; Kim, C.J.; Attinger, D. Boiling Heat Transfer on Superhydrophilic, Superhydrophobic, and Superbiphilic Surfaces. *Int. J. Heat Mass. Tranf.* **2013**, *57*, 733–741. [CrossRef]
26. Xu, W.; Leeladhar, R.; Tsai, Y.-T.; Yang, E.-H.; Choi, C.-H. Evaporative Self-Assembly of Nanowires on Superhydrophobic Surfaces of Nanotip Latching Structures. *Appl. Phys. Lett.* **2011**, *98*, 073101. [CrossRef]
27. Lee, S.; Kim, W.; Yong, K. Overcoming the Water Vulnerability of Electronic Devices: A Highly Water-Resistant ZnO Nanodevice with Multifunctionality. *Adv. Mater.* **2011**, *23*, 4398–4402. [CrossRef] [PubMed]
28. De Angelis, F.; Gentile, F.; Mecarini, F.; Das, G.; Moretti, M.; Candeloro, P.; Coluccio, M.L.; Cojoc, G.; Accardo, A.; Liberale, C. Breaking the Diffusion Limit with Super-Hydrophobic Delivery of Molecules to Plasmonic Nanofocusing SERS Structures. *Nat. Photon.* **2011**, *5*, 682–687. [CrossRef]
29. Jung, S.; Tiwari, M.K.; Poulikakos, D. Frost Halos from Supercooled Water Droplets. *Proc. Natl. Acad. Sci. USA* **2012**, *109*, 16073–16078. [CrossRef] [PubMed]
30. Cassie, A.B.D.; Baxter, S. Wettability of Porous Surfaces. *Trans. Faraday Soc.* **1944**, *40*, 0546–0550. [CrossRef]
31. Vasileiou, T.; Gerber, J.; Prautzsch, J.; Schutzius, T.M.; Poulikakos, D. Superhydrophobicity Enhancement through Substrate Flexibility. *Proc. Natl. Acad. Sci. USA* **2016**, *113*, 13307–13312. [CrossRef] [PubMed]
32. Gilet, T.; Bourouiba, L. Fluid Fragmentation Shapes Rain-Induced Foliar Disease Transmission. *J. R. Soc. Interface* **2015**, *12*, 20141092. [CrossRef] [PubMed]
33. Ina, R.; James, W.; Reza, R.; Thomas, B.; Sachin, K.; Ramesh, J. Nanoindentation Measurements of Teflon-AF Nanosheets. *J. Appl. Polym. Sci.* **2015**, *132*, 41360.
34. Ramimoghadam, D.; Hussein, M.; Taufiq-Yap, H. The Effect of Sodium Dodecyl Sulfate (SDS) and Cetyltrimethylammonium Bromide (CTAB) on the Properties of ZnO Synthesized by Hydrothermal Method. *Int. J. Mol. Sci.* **2012**, *13*, 13275–13293. [CrossRef] [PubMed]
35. Kołodziejczak-Radzimska, A.; Jesionowski, T. Zinc Oxide—From Synthesis to Application: A Review. *Materials* **2014**, *7*, 2833–2881. [CrossRef] [PubMed]
36. Rahman, M.Y.A.; Umar, A.A.; Taslim, R.; Salleh, M.M. Effect of Surfactant on the Physical Properties of Zno Nanorods and the Performance of Zno Photoelectrochemical Cell. *J. Exp. Nanosci.* **2015**, *10*, 599–609. [CrossRef]
37. Usui, H. The Effect of Surfactants on the Morphology and Optical Properties of Precipitated Wurtzite ZnO. *Mater. Lett.* **2009**, *63*, 1489–1492. [CrossRef]

38. Jin, C.; Li, J.; Han, S.; Wang, J.; Sun, Q. A Durable, Superhydrophobic, Superoleophobic and Corrosion-Resistant Coating with Rose-Like ZnO Nanoflowers on a Bamboo Surface. *Appl. Surf. Sci.* **2014**, *320*, 322–327. [CrossRef]

39. Wang, C.-F.; Tzeng, F.-S.; Chen, H.-G.; Chang, C.-J. Ultraviolet-Durable Superhydrophobic Zinc Oxide-Coated Mesh Films for Surface and Underwater–Oil Capture and Transportation. *Langmuir* **2012**, *28*, 10015–10019. [CrossRef] [PubMed]

40. Shaban, M.; Mohamed, F.; Abdallah, S. Production and Characterization of Superhydrophobic and Antibacterial Coated Fabrics utilizing ZnO Nanocatalyst. *Sci. Rep.* **2018**, *8*, 3925. [CrossRef] [PubMed]

41. Wenzel, R.N. Resistance of Solid Surfaces to Wetting by Water. *Ind. Eng. Chem.* **1936**, *28*, 988–994. [CrossRef]

42. Bhushan, B.; Nosonovsky, M. The Rose Petal Effect and the Modes of Superhydrophobicity. *Philos. Trans. R. Soc. A* **2010**, *368*, 4713–4728. [CrossRef] [PubMed]